



Università degli Studi di Napoli Federico II

DOTTORATO DI RICERCA IN

FISICA

Ciclo XXXIII

Coordinatore: Prof. Salvatore Capozziello

A portable EEG-BCI framework enhanced by machine learning techniques

Settore Scientifico Disciplinare INF/01

Dottorando

Pasquale Trinchese

Tutori

Prof. Giovanni Acampora
Dr. Autilia Vitiello

2018/2021

CONTENTS

Introduction	iii
1 Brain Computer Interfaces	1
1.1 A description of the human brain	1
1.2 Neuroimaging techniques	4
1.2.1 SPECT	4
1.2.2 PET	4
1.2.3 MEG	4
1.2.4 fMRI	5
1.2.5 fNIR	5
1.2.6 ECoG and Single-unit recording	5
1.2.7 EEG	6
1.3 Brain signals	6
1.3.1 Evoked signals	6
1.3.2 Spontaneous signals	7
1.4 Direct brain-computer communication	8
1.4.1 BCI classification	9
1.4.2 EEG based BCIs	9
1.4.3 Performance indicators	10
1.5 Machine learning	10
1.6 Applications and future directions	11
2 The EEG-BCI prototype	13
2.1 Concept design	13
2.2 Hardware components	14
2.2.1 Headset	14
2.2.2 Acquisition unit	16
2.2.3 Processing unit	16
2.2.4 Stimulation platform	18
2.3 Firmware	18

2.3.1	Raw-data acquisition module	18
2.3.2	Preprocessing module	19
2.3.3	Classification module	20
3	System Validation	25
3.1	Train-based system validation	25
3.1.1	Dataset acquisition	25
3.1.2	Validation procedure	26
3.1.3	Results	28
3.2	Trainless system validation	32
3.2.1	Dataset acquisition	32
3.2.2	Validation procedure	32
3.2.3	Results	34
4	Applications	37
4.1	Smart wheelchair	37
4.1.1	Architecture	38
4.2	Virtual reality	39
4.2.1	Architecture	39
4.3	Robotic arm control	42
4.3.1	Architecture	42
4.3.2	Live tests	43
	Conclusions	47
	References	49

INTRODUCTION

Brain, in a way quite analogous to the universe, always fascinated humans. Understanding the biological basis of the mental processes that allow us to act, perceive, feel or learn is still a challenge. Although the earliest known studies date back to the time of the ancient Egyptians, only in the twentieth century the technological and scientific progress have provided investigative tools for a deeper understanding of the nervous system. The development of such technologies has also opened the door to active use of brain signals. Such devices, called Brain Computer Interfaces (BCIs), enable direct communication between the brain and external devices. The idea is to record brain waves to define and implement an action using a computer, without depending on the peripheral nervous system and musculature. A typical BCI system is made up of several modules which include signal acquisition, preprocessing, feature extraction, classification and control. Initial research regarding BCIs aimed to provide improved capabilities to impaired users, but, more recently, these techniques are gaining attention also as new means to interact with computers and other devices for healthy subjects too.

BCI is classified as an emerging technology with strong market interest, as demonstrated by a research conducted by *Allied Market Research* which estimated a market size of \$1.46 billion in 2019 and is expected to reach \$3.85 billion by 2027. According to Gartner's Hype Cycle for emerging technologies, BCI will reach its plateau of productivity in 5-10 years. The main challenge is to improve its usability outside the laboratories, thus creating cost-effective, non-invasive but still high-performance devices. In this regard, the most suitable approach is based on electroencephalography (EEG).

EEG extracts brain information in the form of electrical potentials detected through the use of electrodes positioned on the scalp, in a non-invasive way, and is characterized by high flexibility and excellent spatial and temporal resolutions. EEG-based BCIs are able to record both spontaneous signals, generated voluntarily by users, and evoked signals, induced un-

consciously by the influence of external stimuli. Among the various types of evoked signals, Steady-State Visual Evoked Potentials (SSVEPs), produced in the visual cortex area when the subject observes periodic stimuli, have attracted the interest of many researchers due to the high information transfer rate and the little training requirement.

The main drawbacks in EEG-based BCIs are related to the type and number of electrodes used for acquisition. The so called wet electrodes offer better signal quality, but require user maintenance as they dry quickly. Dry electrodes, on the other side, do not require extra intervention, but provide a weaker, noisy signal very sensitive to the environment. A large number of electrodes can compensate for signal weakness, but would not be comfortable and of practical use.

In this work, a single-channel BCI prototype based on EEG and SSVEP signals is presented, addressing the described challenges and providing solutions based on machine learning techniques. Specifically, the research is aimed at the realization, characterization and optimization of a BCI having the following characteristics:

1. *Ease of use*: The system should be up and running quickly, with little or no need for physical device configuration or user intervention.
2. *Single-channel*: The device may be worn for a long time. Using a single channel with a few dry electrodes is less bulky and more flexible and comfortable.
3. *Fast training*: There are several devices where the training may require a very long time (days or weeks) resulting very frustrating for the end user.
4. *Fast response*: In order to be of practical use, the system should provide a control command within few seconds.
5. *Cost-effective*: The device must be accessible to everyone.
6. *Low power consumption*: Since the proposed prototype is wearable, it requires a rechargeable battery. For this reason the components must be chosen with the lowest possible energy consumption.

The listed requirements can be thought as the core features for a minimum viable product. Although the isolated characteristics have been met in literature, there are currently no BCI frameworks, to the best of my knowledge, that satisfy them all.

The thesis roadmap is organized in five chapters.

In the first chapter the reader will become familiar with the physiology of the brain, the associated signals and the main acquisition techniques. The essential elements of a BCI system and the combined use of machine learning are introduced, as well as possible applications.

In the second chapter the developed EEG-based BCI prototype is presented, from the concept design, to the hardware realization up to the integration of the firmware.

The characterization, optimization and validation of the prototype is reported in chapter 3.

In chapter 4, some applications of the developed prototype are presented. Finally, the thesis concludes with various considerations on the potential of the novel framework.

Chapter 1

BRAIN COMPUTER INTERFACES

The advance in the neuroscience field is dictated by the technological progress and, so far, a great variety of cerebral activities have been successfully associated to precise tasks and behaviors. This allowed to develop specific monitoring systems to detect brain dysfunctions, on one hand, and controlling systems to translate brain activities into external commands on the other hand. Instruments capable of transforming brain signals directly into commands go under the name of Brain Computer Interfaces (BCI).

Before describing the acquisition techniques of brain signals, it is appropriate to analyze the origins and the mechanisms underlying the generation of such signals.

This chapter gives a brief introduction to the human brain, following with a description of the main neuroimaging and readout methods, with their pros and cons. Finally, a description of the key elements of BCI systems, their classification and possible applications in different areas are provided.

1.1 A description of the human brain

The brain is the center of a highly specialized system aimed at managing actions and sensory information dispatching signals to and from various regions of the body. It is part of a more general structure known as nervous system which could be generally divided into two main parts: the central nervous system (CNS) and the peripheral nervous system (PNS). The former comprises the brain and the spinal cord and coordinates the information coming from both the external environment, through sight, taste, hearing, touch and smell, and from the body internal system. The latter consists of nerves and ganglia and serves as a relay between the CNS and the rest of the body.

The fundamental unit of the nervous system is the neuron, a special cell that can actively process electrical signals. The main elements that characterize a neuron are shown in Fig 1.1. Starting from the main cell body, called soma, cytoplasmic extensions originate. Input-type extensions are called dendrites. They are sensitive to environmental alterations or to the activities of neighboring cells and propagate electrical signals towards the soma. In particular conditions, generally a threshold process, the neuron generates an impulse known as *action potential*, which propagates through a single output extension, the axon, that takes care to transmit information to different neurons, muscles and glands through the synaptic terminations. From a physiological point of view, action potentials represent a

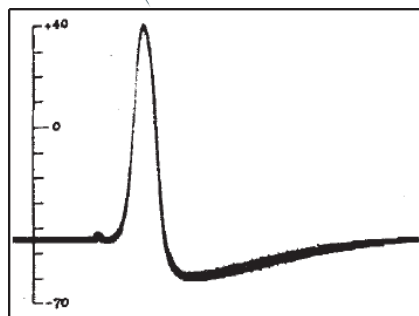
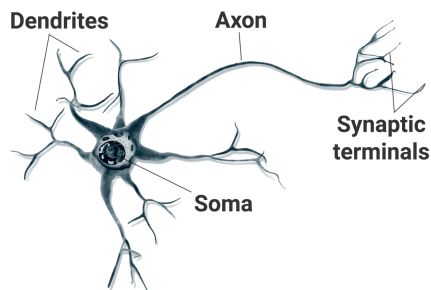


Fig. 1.1: Top: Anatomy of a neuron. Bottom: First intracellular measurement of an action potential [1].

modification of the neuron's membrane conductance. In stationary conditions, the potential difference between the inside and outside of the cell membrane is on average -70 mV , due to the different concentration of intra- and extra- membrane ions (in particular Na^+ and K^+). The flux of ions across the cell membrane is regulated by glyco-protein macromolecules known as ion channels. In neurons, the ion channels are normally closed and do not allow the passage of ions. If an adequate stimulus causes a change in the membrane potential above a critical value then the channels open allowing the transition of ions across the membrane, i.e., the membrane conductance increases and the action potential is triggered. An example of an action potential observed with an oscilloscope is shown in Fig. 1.1. The whole process takes place in few milliseconds.

The human brain approximately contains $21 - 26 \times 10^{12}$ neurons [2], organized in an apparent chaotic network capable of processing extremely complex information. Two main regions can be identified in the brain: the cerebral cortex, responsible for high level functions such as reasoning, language processing and visual analysis, and the sub-cortical regions which regulate the vital functions such as respiration and heart rate.

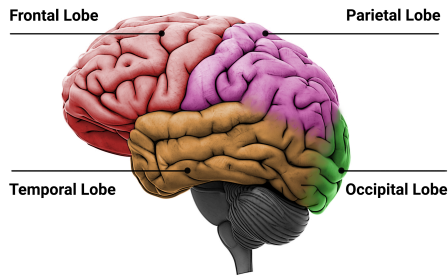


Fig. 1.2: Lobes of cerebral cortex.

The cerebral cortex arouses a lot of interest in the world of research as its functions are essentially linked to the will of the person, an essential requirement for the development of brain-computer interfaces (BCIs). The functioning of the cerebral cortex is still unclear, however, since the mid-nineteenth century, many studies [3, 4] have shown that a certain amount of cortical functions are localized.

The concept of localization should not be intended in the strict sense, but as areas in which brain activity is more intense during certain actions.

The cerebral cortex is a bilateral structure consisting of two hemispheres, each of which can be divided into four lobes (Fig. 1.2). The frontal lobe is primarily responsible for voluntary movement, attention and problem solving. The parietal lobe is mainly responsible for spelling, perception and spatial awareness. The temporal lobe is connected to memory, learning, language, emotional control. Finally, the occipital lobe is related to the interpretation of visual stimuli. A particular characteristics in the organization of the cerebral cortex is that each hemisphere is related to the processes on the opposite side of the body. Starting from the division into lobes, much more detailed and localized functional maps of the brain were subsequently proposed. In particular, the Brodmann map identifies 52 different areas (Fig. 1.3), each one devoted to a specific function. However, it should be noted that small lesions to the cerebral cortex do not impair its normal functioning, which highlights an extremely flexible neural organization.

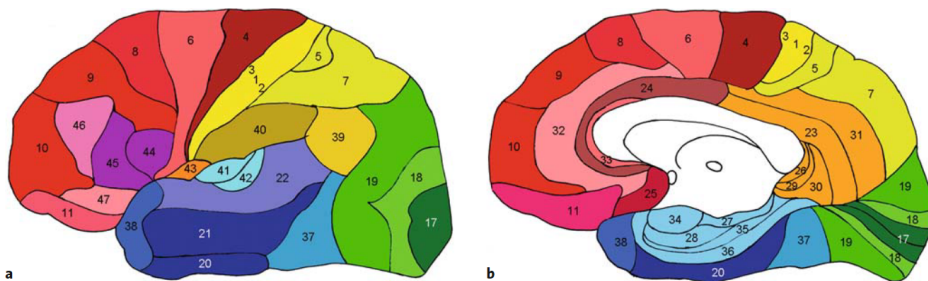


Fig. 1.3: Illustration of Brodmann's cortical maps. Lateral (a) and medial surface (b).

Source: [5]

1.2 Neuroimaging techniques

The neural activity of the brain can be analyzed using different methods and tools. The main techniques for detecting, displaying and interpreting such activity are described below.

1.2.1 SPECT

Single Photon Emission Computerized Tomography (SPECT) is an imaging method based on the tracking of gamma rays emitted by radioactive nuclei injected into the patient's bloodstream. To identify particular areas, specific chemical compounds are used so that there is a greater accumulation of radionuclides in the affected areas. A commonly used radioactive tracer is the metastable nuclear isomer of technetium ^{99m}Tc . Using position sensitive photodetectors (typically rotating cameras) 3D images of the part of the brain under examination can be generated. SPECT devices have a spatial resolution of about 1 *cm* and a temporal resolution of several seconds. Better spatial resolutions can be achieved with the use of new detectors such as silicon photomultipliers [6].

1.2.2 PET

Positron Emission Tomography (PET) is in principle very similar to SPECT. It is also based on gamma ray tracking. However, radionuclides do not directly emit photons but positrons, which in turn interact with the electrons surrounding the affected area [7]. From this interaction two annihilation photons are emitted in opposite directions which, once detected in time-coincidence window, allow to generate an image in a similar way to SPECT. PET can reach spatial resolutions of less than a millimeter but it is very expensive and is only present in specialized centers.

1.2.3 MEG

Magnetoencephalography (MEG) is a non-invasive technique used to measure the weak magnetic fields produced by the synchronous activity of thousands of neurons in the brain. These fields allow to trace the brain region activated by an external stimulus or to identify injured areas. The detection is based on superconducting quantum interference devices (SQUID) which convert magnetic waves into electrical signals [8].

1.2.4 fMRI

Functional Magnetic Resonance Imaging (fMRI) is used to measure changes in blood oxygen levels in active areas of the brain. This phenomenon is known as blood oxygenation level dependent (BOLD) and is detected by placing the patient in a strong static magnetic field. In this situation, the spins of certain nuclei (including hydrogen) show a precession motion around the magnetic field vector at a fixed frequency. By applying radio frequency pulses, the directions of the spins can be brought in a direction perpendicular to the magnetic field by inducing a voltage variation in a receiving circuit through antennas placed around the area to be imaged [9]. fMRI produces high spatial resolution but a very poor temporal resolution.

1.2.5 fNIR

Functional Near Infrared (fNIR) imaging is a fairly recent technology based on the projection of infrared light at different wavelength into the brain. The re-emitted light allows to determine the oxygen concentration, which modifies the scattering and absorption properties, in the areas of interest [10]. In this way, images similar to fMRI can be obtained with better spatial resolution at the expense of temporal resolution.

1.2.6 ECoG and Single-unit recording

Electrocorticography (ECoG) allows to measure brain activity through surface electrodes placed on the cerebral cortex [11, 12]. It is a method with extremely high spatial and temporal resolutions since neural electrical activity is detected directly on the surface of the brain. Recent studies have shown that using micro surface electrodes ($< 100 \mu m^2$) it is possible to record single-neuron activity [13]. However, being invasive and limited to the exposed area of the brain, it still has no practical use outside laboratories. Superior performances can be achieved with intracortical electrodes, known as single-unit recording devices. However, they have even greater limitations, such as damage to the blood brain barrier and allergic reactions.

unconscious way. Although external stimuli can sometimes be uncomfortable, evoked signals have the advantage that they require little user effort and do not present substantial differences from subject to subject. The most known evoked signals are Steady State Evoked Potentials (SSVEP) and P300.

SSVEP

Steady State Visual Evoked Potentials (SSVEP) are rhythmic variations of electrical potential produced on the primary visual cortex, in correspondence of the occipital lobe (Fig. 1.2). They can be evoked through periodic visual stimuli and are characterized by a response frequency equal to that of stimulation. Stimuli can be generated by light flashes or flickering images projected on a display. Due to their high signal to noise ratio (SNR) and fast time response, SSVEPs are ranked among the fastest and most immediate signals currently available [16].

P300

P300 is a peak in the detected signal that appears about 300 *ms* after the subject has been exposed to an infrequent or unexpected stimulus. An example is the repetition of a sequence of random stimuli with a less frequent one [17]. As for the SSVEPs, the P300 also does not require user training but is very tiring and repetitive.

1.3.2 Spontaneous signals

Spontaneous signals are generated voluntarily by the subject and are mostly based on cognitive tasks such as music imagination, mathematical calculation or movement simulation. The user mentally simulates a process, then pattern analysis is performed on the recorded signals with more or less sophisticated techniques, including machine learning. Among the various spontaneous signals related to cognitive tasks, motor imagery and slow cortical potentials are the most used.

Motor imagery

Motor imagery is a mental task in which the subject imagines making a movement, such as hand or foot movements, without actually doing it. Such tasks imply a change in the amplitude of brain signals coming from

the motor cortex, known as sensorimotor rhythms, which can be detected and used as control signals [18]. Indeed, motor imagery is very suitable for control applications but needs several electrodes for good performances and may require long training time.

Slow cortical potentials

Slow cortical potentials (SCP) are slow variation of brain activity controlled by an individual using operant conditioning. These signals occur in the central and frontal part of the cortex and can encode various cognitive parameters such as those related to movements or language [19]. It may require very long training time and some users may not be able to generate these signals.

1.4 Direct brain-computer communication

The first person to highlight the possibility of direct communication between computer and brain, in particular through EEG, was Jacques J. Vidal in 1973 on the basis of the state of the art of technologies and neurophysiology at that time [20]. He was also the first to refer to Brain Computer Interfaces (BCI) as systems capable of acquiring brain signals to voluntarily control external devices. The realization of a BCI system must include some essential elements. These are summarized in the flowchart shown in Fig. 1.5. Starting from the user, brain signals are acquired through an headset hosting the acquisition sensors. Signals are subsequently filtered, digitized, and preprocessed by a microcontroller to reduce the background noise and extract the main features, i.e., the extraction of information through various processing techniques, such as spectral or time-frequency analysis. The processed signals are then transferred to a recognition software which performs a classification, interpreting the characteristics extracted from the signal. Finally, the recognized patterns are translated into

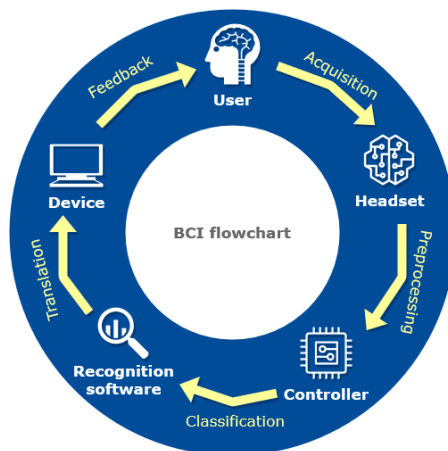


Fig. 1.5: Basic flowchart of a Brain Computer Interface.

commands for controlling external devices. It is also necessary that feedback is provided to the user so that he is aware of the performed action.

1.4.1 BCI classification

Besides the distinction between invasive and non-invasive BCIs, which depends on the particular neuroimaging technique chosen, BCI systems can be classified according to the degree of user interaction and synchronization.

Dependent and independent BCI

Dependent BCIs require a minimum of motor control of the subject's sensory muscles. For example, such a system might require the user to focus on various external stimuli to activate related brain signals. Independent BCIs, on the other hand, does not require any motor control.

Synchronous and asynchronous BCI

In synchronous BCIs, the user can interact with the system only in predetermined time intervals. Outside these time windows the system would not work. In asynchronous BCIs, also called self-paced, the system is able to respond to the mental tasks of the subject at any time.

1.4.2 EEG based BCIs

The most suitable neuroimaging methods for a BCI system are ECoG, single-unit recording and EEG, as they offer far superior spatial and temporal resolutions and are also less bulky. Among these three, EEG is of particular interest as it does not require a cranial opening to place the electrodes and the entire acquisition and processing system could be embedded into the headset. The main drawback in using an EEG-BCI system is related to the application of many electrodes on the scalp for adequate signal recognition, resulting very uncomfortable and not practical. This problem can be addressed by using machine learning techniques to extrapolate useful information using only few channels, especially when many classes (the number of different outcomes that a signal is expected to encode) are involved.

1.4.3 Performance indicators

Different indicators can be taken into consideration when comparing different BCI systems, although, depending on the type of application, one quality may be preferred over another. The most used performance indicators are:

- *Detection accuracy*. It is the ratio of correctly predicted classes to the total number of predictions made:

$$accuracy = \frac{n_correct_predictions}{n_total_predictions} \quad (1.1)$$

The accuracy strongly depends on the Signal-to-Noise ratio (SNR) i.e., the ratio of signal power to the background noise power.

- *Detection time*. It can be defined as the mean time elapsed between two consecutive correct predictions.
- *Information transfer rate (ITR)*. It is the amount of information transferred per unit time (precisely, bit per minutes). It takes into account the detection accuracy, detection time, and the number of classes [21]. Formally:

$$ITR = Q \times \left[\log_2 N + P \times \log_2 P + (1 - P) \times \log_2 \left(\frac{1 - P}{N - 1} \right) \right] \quad (1.2)$$

where N is the number of target or classes, P is the detection accuracy and Q is the detection time in minutes.

1.5 Machine learning

Machine learning (ML) refers to a set of classification techniques that allows to obtain information on complex data whose characteristics are not fully known. In particular, ML is a branch of artificial intelligence that aims to build a model starting from data samples, known as training data, in order to make predictions on new data. Indeed, dataset preparation is the most crucial aspect in machine learning. A training dataset is made of vectors, whose dimension depends on the number of unique measurable properties of the study under consideration. These properties are known as *features* and the resulting vector is called *feature vector*. Usually, features are extracted from raw data on the basis of statistical considerations, or

even hypotheses, on the observed phenomena. The techniques for manipulating raw data in order to extract relevant features are known as pre-processing algorithms. Each training vector has an associated label that points to the set of possible *classes* to which a vector can belong. The set of classes is usually discrete but can also belong to a subset of real numbers. The dataset made up of feature vectors, with the associated classes, allows to train a model capable of predicting which class new input vectors belong.

Machine learning is particularly suitable for the classification of brain signals as they are often very noisy and not much is known about them. Patterns can be very hidden and extremely difficult to detect with classical signal analysis. The techniques used in this work will be described in the next chapter alongside the description of the developed BCI prototype.

1.6 Applications and future directions

Being both a monitoring and control device, the possible applications of BCIs are innumerable. These includes, but not limited to:

- the study and monitoring of particular disorders (epilepsy, sleep disorders)
- rehabilitation from neurodegenerative diseases
- support for paralyzed patients
- control of prostheses or commonly used devices
- performance enhancement
- videogames controller
- augmented and virtual reality assistance

For each area of application, it is essential to improve its usability and make it accessible to everyone. For these reasons, the research objectives of this work are pursued by constantly taking into account the key properties for the BCIs of the future: ease of use, rapid training, fast response, integrated analysis, cost effectiveness, and low power consumption. In this work a BCI prototype having the mentioned characteristics is proposed. A detailed description is provided in the next chapter.

Chapter 2

THE EEG-BCI PROTOTYPE

Based on the considerations addressed in the previous chapter and thanks to the collaboration with QUASAR of the physics department of the Federico II University of Naples, the electronic engineering department, the Protom Group S.p.A. and the collaboration with the CERN robotics group, I have developed a wearable single-channel BCI prototype based on electroencephalography specific for SSVEP signals. The prototype has been thought to meet the usability and low-cost requirements. For this reason components have been chosen to have a balanced ratio between costs and performances. Its realization involved hardware configuration, software development as well as 3D modeling and printing. A detailed description is provided throughout this chapter.

2.1 Concept design

As delineated in the previous chapter, SSVEP signals result as response to periodic visual stimuli, such as flickering lights or images. These signals can be analyzed to recognize which stimulus the subject is focusing on, paving the way for a control system in various applications.

The concept design of the developed system is shown in Fig. 2.1. A device renders the visual stimuli, eliciting SSVEP responses in the subject. Signals are captured through EEG electrodes positioned on the scalp, digitized by the acquisition unit and sent to the processing unit. Here signals undergo segmentation, filtering and transformations, such that the relevant features are extracted and classified according to the observed stimulus. The system also integrates a server that can send commands to external devices based on the outcomes of the classification.

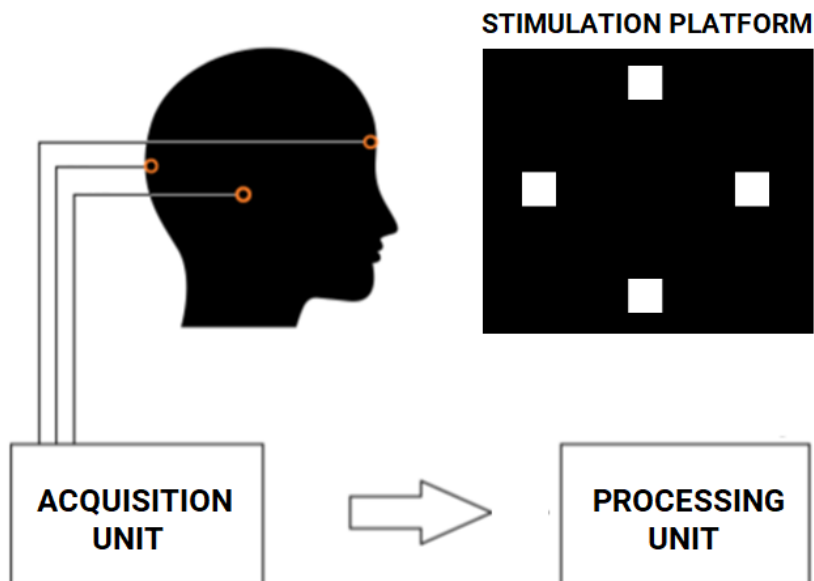


Fig. 2.1: Concept design of the proposed EEG-BCI prototype.

2.2 Hardware components

The proposed prototype is made of four fundamental units: the headset, the acquisition unit, the processing unit and the stimulation platform. I will not provide hardware details on the stimulation platform in this section as there may be of different types and the system allows for quick configuration. The particular platform used will be described in chapters 3 and 4 along with the type of application covered.

2.2.1 Headset

The headset design has been thought to host the electrodes in the occipital zone (Oz) and the frontal-parietal zone (Fpz) according to the 10/20 system. In fact, the Oz position is located in correspondence of the visual cortex, where SSVEP signals are more intense. Since the captured signal is the voltage difference between the two electrodes (Sec. 2.2.2), the Fpz position is strategic as it is as far as possible from Oz, avoiding signal overlapping.



Fig. 2.2: 3D model of the headset, on the left, and 3D printed headset hosting the electrodes, on the right.

Electrodes

The adopted electrodes are of two types, passive and active. Precisely, two active electrodes have been used for signal detection and a passive Driven Right Leg (DRL) electrode used as a reference electrode. The passive electrode simply consists of a gold-plated flat surface assembled with a shielded cable. The active ones contain a preamplification circuit that improves the signal and reduces environmental noise. One of the two active electrodes has been modified by adding twelve gold-plated spring connectors to improve the skin contact through the hair.



Fig. 2.3: Gold-plated flat electrode on the left and a modified spring-loaded electrode on the right.

2.2.2 Acquisition unit

The acquisition unit is based on the Olimex EEG-SMT (Fig. 2.4), a 10-bit, 256 Hz, 2-channels, differential input Analog-Digital Converter (ADC) for digitizing brain signals. Three electrodes have been used as input to the Olimex, two active electrodes for the differential ADC and a passive one as reference electrode. The ADC digitizes data as an integer number ranging from 0 to 1023 with a dynamic range of ± 0.39 mV due to the default internal gain of the device ($G = 6427$).

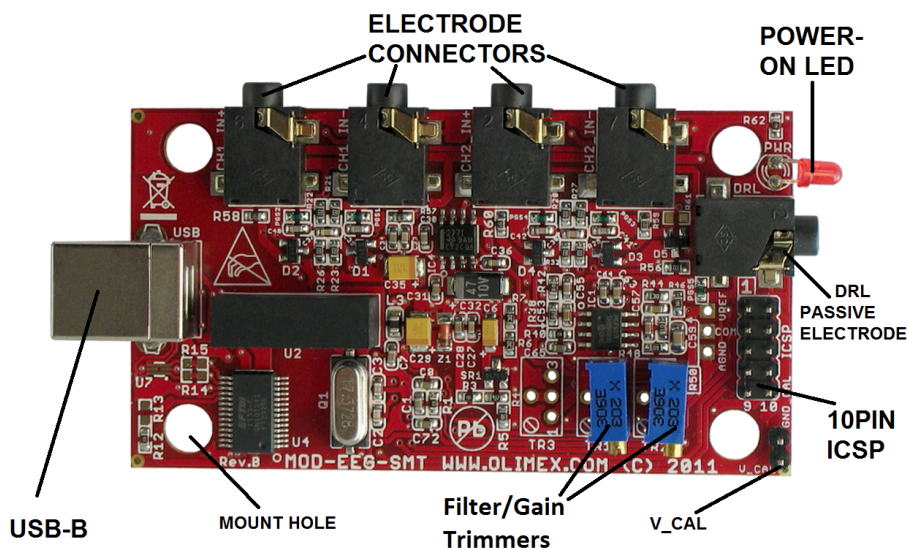


Fig. 2.4: Olimex EEG-SMT.

2.2.3 Processing unit

The processing unit is built upon a Raspberry Pi 3 single-board computer (Fig. 2.5), developed by the Raspberry Pi Foundation, with a $4 \times$ ARM Cortex-A53 1.2GHz CPU, 1GB RAM, several multipurpose pins and peripherals, wireless network capabilities such as Bluetooth and WiFi, and a Debian-based Linux operating system installed. It communicates via USB with the Olimex device, integrates preprocessing and classification algorithms for the digitized data, and serves as WiFi interface to interact with external devices.

Both the acquisition unit and the processing unit have been packed together in a 3D printed box that can be worn with a belt (Fig. 2.6). The

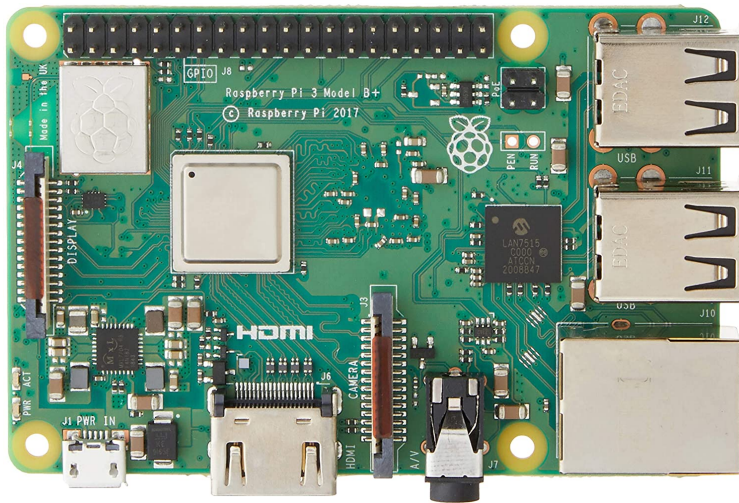


Fig. 2.5: A Raspberry Pi 3 single-board computer used as processing unit and as WiFi interface.

box also contains a slot for a powerbank capable of powering the system for about three hours.



Fig. 2.6: The EEG prototype packed into the 3D printed wearable box.

2.2.4 Stimulation platform

The stimulation platform consists of a display capable of providing visual stimuli, usually black-white squares oscillating on a black background. The display can be from a laptop, a tablet, a smartphone or virtual- and augmented-reality headsets. Flickering frequencies values depend on the device. In fact, the number of the producible frequencies are limited to integer divisors of the monitor refresh rate [22]. To overcome the limits imposed by the refresh rate a pulsed sinusoidal modulation of the brightness can be used.

If f is the desired frequency and R the refresh rate of the device, the brightness of the stimulus at the frame index n is given by:

$$S(n, f) = \sin\left(\frac{2\pi f n}{R}\right) \quad (2.1)$$

The pulsed sinusoidal waveform is obtained by replacing all negative values with zero.

2.3 Firmware

The main firmware is entirely written in Python and hosted on the Raspberry Pi 3. It comprises a set of methods accessible through an integrated HTTP server. Each method calls a sub-module responsible for a precise task, from data acquisition to the prediction algorithms. The main modules are three: raw-data acquisition, preprocessing and classification.

When a request is sent to the server, sampled data is processed in order to provide either the predicted frequency (using the train-based or the train-less algorithms) or the estimated number of eyeblinks. The flowchart of the server is shown in Fig. 2.7 showing the main requests. Other requests allow the user to choose the prediction algorithm, obtain raw data, and save trained models.

2.3.1 Raw-data acquisition module

This method continuously fill a built-in 4096 words buffer, following the First-In-First-Out (FIFO) paradigm, retrieving digitized data from the Olimex EEG-SMT acquisition unit. The buffer size corresponds to the last 16 s of data that will be immediately available for computation. This module runs on a separate thread (Fig. 2.7).

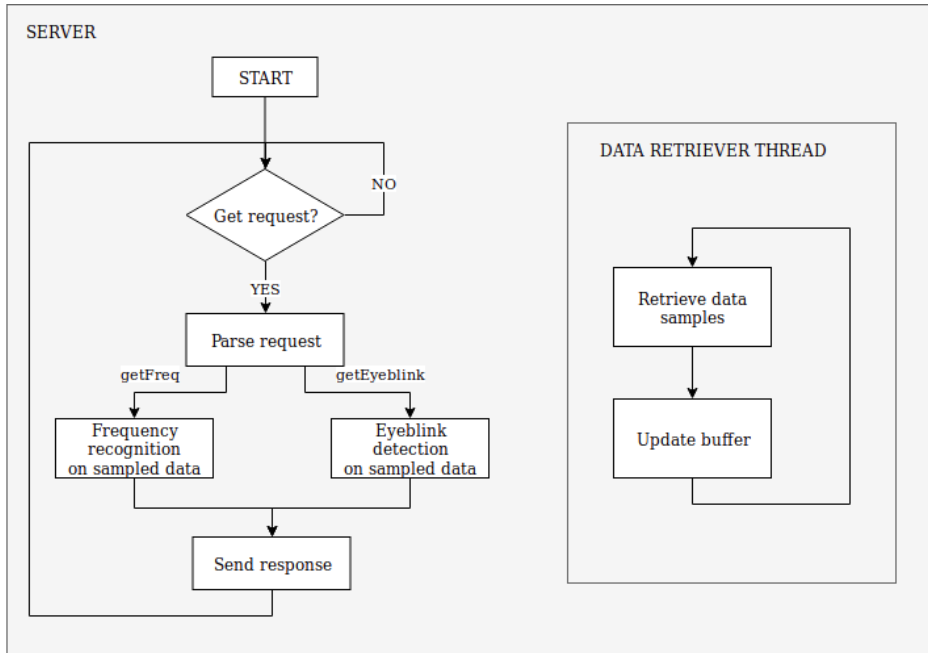


Fig. 2.7: Flowchart of the Raspberry Pi server.

2.3.2 Preprocessing module

Includes a set of analysis tools used to extract relevant features for the final classification. Such tools are:

- Segmentation: produces signal segments of fixed length, known as *time window*. Segments can share a portion of the original signal (*overlap*) with a settable percentage.
- Fast Fourier Transform (FFT): invented by Gauss in 1805 and rediscovered later by Cooley-Tukey [23], is a powerful tool that converts signal segments from the time domain to the frequency domain. Its numerical expression is:

$$X_q = \sum_{k=0}^{N-1} x_k e^{-i \frac{2\pi kq}{N}} \quad (2.2)$$

where q ranges from 0 to $N - 1$, x_0, \dots, x_{N-1} are the elements of the input buffer, N its length, and X_0, \dots, X_{N-1} are complex numbers constituting the transformed signal.

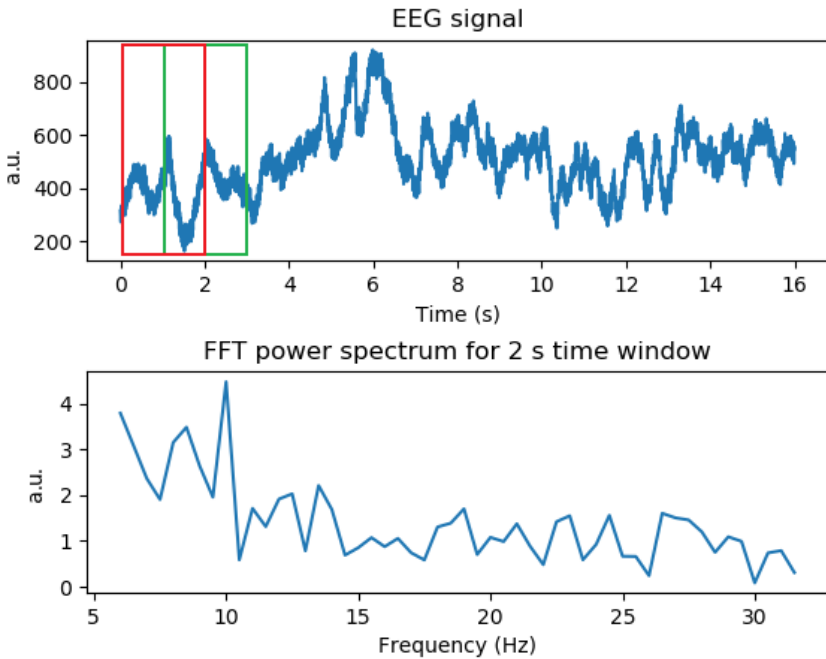


Fig. 2.8: EEG recording with an example of 2 s windowing, 50% overlap, and the FFT power spectrum for the first 2 s time window, in the range 4 Hz - 32 Hz.

- Butterworth passband filter: a signal filter designed to attenuate unwanted frequencies and have a frequency response as faithful as possible in the chosen passband.
- Normalization: scales data into a range of $[0, 1]$.
- Standardization: scales data to have a mean of 0 and a standard deviation of 1.

2.3.3 Classification module

Performs frequency prediction and eyeblink recognition on the preprocessed data. Three submodules have been implemented:

Train-based algorithms

Include a set of interchangeable machine learning algorithms to perform classification. A training phase is needed before being able to use the system. The implemented machine learning algorithms are:

- *Logistic Regression* (LR): a machine learning technique that uses a logistic function to describe the outcomes of a binary variable. More in detail, the logistic function is a sigmoid function,

$$\sigma(t) = \frac{1}{1 + e^{-t}} \quad (2.3)$$

which takes as input a real value t and maps it in the $(0, 1)$ interval. Given a vector \vec{x} , t can be expressed as a linear combination of the vector components x_1, \dots, x_N . Formally,

$$t = \omega_0 + \omega_1 x_1 + \dots + \omega_N x_N \quad (2.4)$$

In this way, the logistic function can be rewritten as follows:

$$p(\vec{x}) = \sigma(t) = \frac{1}{1 + e^{-(\omega_0 + \omega_1 x_1 + \dots + \omega_N x_N)}} \quad (2.5)$$

where $p(\vec{x})$ is interpreted as the probability that a particular sample belongs to the positive class. The aim of LR is to find the best coefficients $\omega_0, \dots, \omega_N$ that fit data to the probability distribution. The regression coefficients are estimated using the maximum likelihood estimation [24].

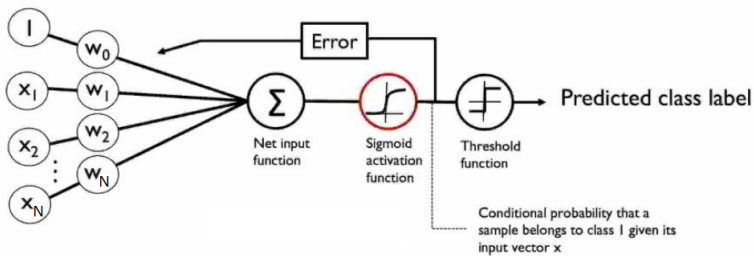


Fig. 2.9: Schematic of a Logistic Regression classifier [25].

- *Support Vector Machines* (SVM): a binary classifier that finds an optimal hyperplane that separates each class in a high dimensional mapping of the features space [26]. In detail, given a set of labeled training instances $(\mathbf{x}_1, y_1), \dots, (\mathbf{x}_l, y_l)$ with $\mathbf{x}_i \in \mathbb{R}^n$ and $y_i \in \{-1, 1\}$, SVM requires the minimization of

$$\frac{1}{2} \mathbf{w}^2 + C \sum_{i=1}^l \xi_i \quad (2.6)$$

subject to the constraints

$$y_i(\mathbf{w} \cdot \phi(\mathbf{x}_i) + b) \geq 1 - \xi_i \quad (2.7)$$

$$\xi_i \geq 0 \quad (2.8)$$

where $\phi : \mathbb{R}^n \rightarrow \mathbb{R}^N$ is a vector function that maps the n -dimensional input vector \mathbf{x} into an N -dimensional feature vector and can be defined by a kernel function $K(\mathbf{x}_i, \mathbf{x}_j) = \phi(\mathbf{x}_i)^T \phi(\mathbf{x}_j)$. C is the penalty parameter (also known as regularization parameter).

Some common kernels are:

- $K(\mathbf{x}_i, \mathbf{x}_j) = \mathbf{x}_i^T \mathbf{x}_j$ (linear)
- $K(\mathbf{x}_i, \mathbf{x}_j) = (\gamma \mathbf{x}_i^T \mathbf{x}_j + r)^d$ (polynomial)
- $K(\mathbf{x}_i, \mathbf{x}_j) = \exp(-\gamma |\mathbf{x}_i - \mathbf{x}_j|^2)$ (radial basis function)

Trainless algorithms

Correlation-based algorithm to distinguish between two classes. Given a signal fragment of length T , Pearson correlation coefficients are evaluated between the filtered data D_T and two sine waveform - $Y_1(\phi)$ and $Y_2(\phi)$ - each with a frequency of the flickering stimuli and variable phase.

The selected correlation coefficients ρ_1 and ρ_2 consist of:

$$\rho_1 = \max_{\phi \in [0, 2\pi[} \frac{\text{cov}(D_T, Y_1(\phi))}{\sigma_{D_T} \cdot \sigma_{Y_1(\phi)}} \quad (2.9)$$

$$\rho_2 = \max_{\phi \in [0, 2\pi[} \frac{\text{cov}(D_T, Y_2(\phi))}{\sigma_{D_T} \cdot \sigma_{Y_2(\phi)}}$$

Then, the following features can be defined:

$$F_A = \max(\rho_1, \rho_2) \quad (2.10)$$

$$F_B = \frac{\max(\rho_1, \rho_2) - \min(\rho_1, \rho_2)}{\min(\rho_1, \rho_2)}$$

Given two threshold values T_A and T_B , a signal fragment can be marked as recognized if:

$$F_A > T_A \wedge F_B > T_B \quad (2.11)$$

If condition 2.11 is not satisfied, an idle status is assigned to the current signal fragment and a new fragment of length T , overlapping with the previous one of $T/2$, is processed. In this way, the response time of the system can be defined as the time interval between two recognized stimuli.

Eyeblink detection

Estimates the number of eyeblinks in a fixed time window. EEG eye-blink artifacts are characterized by huge peaks along the EEG track. Such peaks are first detected when the signal exceeds a fixed threshold, acting as a trigger, then EEG data within 1 s time window is integrated with respect to the signal baseline. In this way, the integrated signal is proportional to the number of eye-blinks occurring in the time window. The baseline is evaluated averaging the first 150 ms signal (pre-trigger) and the last 150 ms of the time window. The trigger threshold was set to 0.2 (normalized units), corresponding to 80% of the average maximum eyeblink amplitudes, based on the previously collected data. In Figure 2.10 are shown two eye-blink artifacts with a graphical explanation of the detection principles.

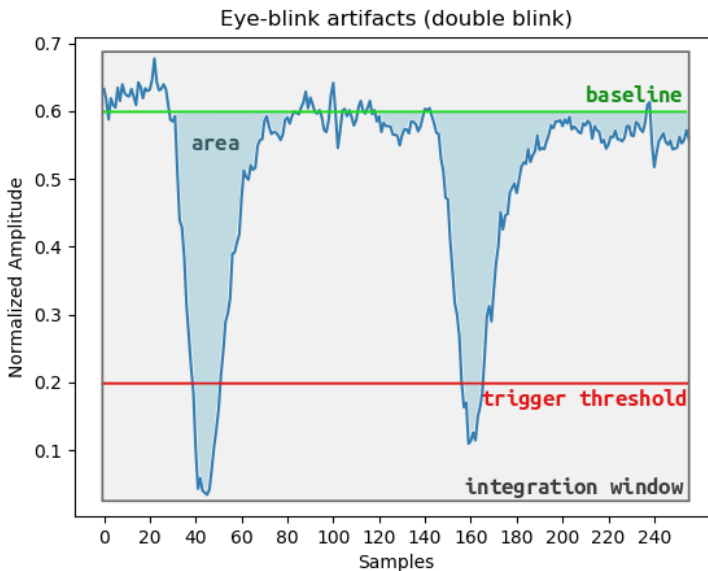


Fig. 2.10: Typical eye-blink artifacts in 1 s time window. When the first peak exceeds the trigger threshold (red line) a 1 s time window starting 150 ms before the trigger is integrated with respect to the baseline (green line). The highlighted area is proportional (within a certain tolerance) to the number of blinks.

The algorithms described in this chapter are integrated into the device, which therefore can also carry out the training part. However, for faster analysis on multiple subjects, the algorithms were trained offline and implemented on the device for online testing. The validation of the prototype is reported in the next chapter.

Chapter 3

SYSTEM VALIDATION

The validation process involved several steps, from data acquisition to the evaluation of the performances of the implemented algorithms. Two datasets were created during the PhD program to test the performances of the proposed algorithms. In particular, a first dataset was acquired to assess train-based algorithms, i.e., using machine learning techniques, on four-classes data. A second collection of data was acquired with a different setup to evaluate the trainless algorithm on two-classes data.

Data acquisition protocols and the experimental setups are described in this chapter for each of the implemented algorithms, evaluated in terms of accuracy and response time.

3.1 Train-based system validation

3.1.1 Dataset acquisition

Experimental setup

Brain signals have been acquired through the single channel EEG-BCI, described in chapter 2, from eleven volunteers aged from 25 to 50 years. Participants were equipped with the 3D printed headset (Sec. 2.2.1) hosting the FPz, Oz and DRL electrodes and seated on a chair 70 cm away from the stimulation platform, consisting of a 15.6" laptop monitor. Stimuli consisted of four alternating black-white 80×80 pixel squares on a black background with flickering frequencies of 8.57 Hz, 10 Hz, 12 Hz and 15 Hz, compatible with the monitor refresh rate.

Experimental protocol

Each volunteer was asked to carry out the following steps:

1. Focus on one stimulus out of four for 16 seconds, as indicated by the software interface.
2. Wait four seconds before focusing on a different stimulus. No stimuli were provided during the 4 seconds break.

The steps were repeated until data related to all four stimuli was acquired. The resulting dataset consisted of 44 recordings of 16 seconds each. Since the ADC sampling rate is 256 Hz, a total of 180224 samples were collected [27].

3.1.2 Validation procedure

To evaluate the performances of the classification algorithms in multiple scenarios, data was segmented using different combinations of two parameters: time windows length and overlap percentages. In particular, five values were considered for the time windows - 2s, 3s, 4s, 5s and 6s - and six values for the overlap percentages - 35%, 50%, 65%, 80%, 90% and 95% -. Feature extraction has been then applied to the obtained dataset. Specifically, each segment was converted from the time domain to the frequency domain using the Fast Fourier Transform (FFT), as explained in Sec. 2.3.2. The power spectrum of the FFT in the range [4Hz, 32Hz] has been used as feature vector. Successively, data were standardized in order to have zero mean and unit variance.

The dataset size for each combination of segmentation parameters are shown in Table 3.1. Since the FFT size is proportional to the number of samples, we also reported in Table 3.2 the number of features for each time window length.

Table 3.1: Dataset size for each combination of time window length (in seconds) and overlap percentage.

Window Size/Overlap	35%	50%	65%	80%	90%	95%
2.0 s	540	702	1003	1755	3510	7020
3.0 s	359	467	668	1168	2337	4673
4.0 s	269	350	500	875	1750	3500
5.0 s	215	280	399	699	1398	2796
6.0 s	179	233	332	582	1163	2327

Table 3.2: Number of features for each time window size.

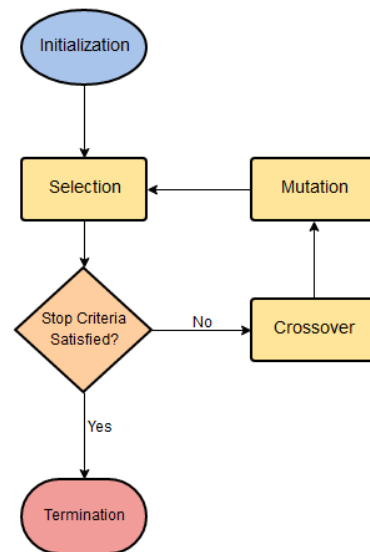
Window Size (s)	# Features
2.0	56
3.0	84
4.0	112
5.0	140
6.0	168

In order to validate the classification algorithms each dataset, resulting from the different combinations of time window and overlap, was randomly partitioned into two subsets, 80% for training the models and the remaining 20% for testing.

The training dataset was evaluated using a classical ten-fold cross-validation procedure.

Two classification algorithms, Logistic Regression (LR) and Support Vector Machines (SVM), explained in Sec. 2.3.3, have been evaluated in terms of accuracy and compared with the state of the state of the art approach for single channel SSVEP-based BCIs, namely the Linear Discriminant Analysis (LDA) [28].

Moreover, the training dataset has been also used for the optimization of the hyper-parameters of SVM by the means of *genetic algorithms*. Genetic algorithms aim to solve an optimization problem by acting on a population of potential solutions and reproducing the natural evolution that leads to the survival of the most suitable individuals able to adapt to environmental conditions [29]. Usually, genetic algorithms operate on encoded representations of solutions, called chromosomes. The algorithm begins with the definition of an initial population of possible solution, usually generated randomly. Each chromosome is evaluated by the means of a *fitness function* that reflects the quality of a solution for the consid-

**Fig. 3.1:** Flowchart of a genetic algorithm.

ered problem. Chromosomes providing the best solutions are selected as parents of the next generation. Successively, parents undergo crossover and mutation to create the new population. In particular, the crossover swaps portions between two randomly selected chromosomes. Mutation causes a random alteration of the chromosome components. The steps described can then be performed again on the new population. The algorithm terminates when specified conditions, such as the maximum number of iterations or a threshold value for the fitness function, are reached.

In our case, the chromosome is represented as a real vector composed of the SVM parameters to be tuned. In detail, the parameters tuned for the SVM classifier are the penalty parameter C , the γ parameter related to the RBF kernel function $K(\mathbf{x}_i, \mathbf{x}_j) = \exp(-\gamma|\mathbf{x}_i - \mathbf{x}_j|^2)$, described in Sec. 2.3.3. The SVM individual is then of the form (C, γ) . The fitness value of a chromosome is defined as the average accuracy calculated by applying the ten-fold cross-validation procedure. The genetic operators applied in each generation are the one-point crossover and the polynomial mutation, with 5% independent probability for each parameter to be mutated. As stop criteria we consider a maximum of 1000 generations [30].

3.1.3 Results

Logistic regression

The first study aimed at evaluating the performance of LR with respect to LDA. We initially evaluated the impact of the overlap percentage on the accuracy of the system. In Figs. 3.2 and 3.3 are shown the accuracy scores achieved by LR and LDA for different time windows and overlap percentages. In particular, Fig. 3.2 shows the accuracy scores of LR obtained by applying the cross validation on the training dataset. Fig. 3.3 shows the same results for the LDA classifier.

Not surprisingly, the best accuracy values are achieved with higher overlap percentages. Consequently, LR and LDA are compared by fixing the 95% overlap percentage, which provided the best results. The results are reported in Figs. 3.4 and 3.5 where are shown, respectively, the accuracy scores of the cross validation applied to the training dataset and the accuracy scores of the trained models on the testing dataset.

The relative improvement of LR with respect to LDA is reported in Table 3.3. The calculated average relative improvement amount to 4.7% [31].

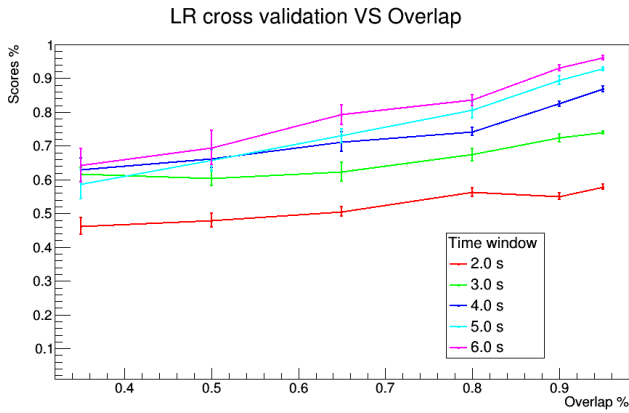


Fig. 3.2: Cross validation accuracy of LR as a function of the overlap percentages for each time window.

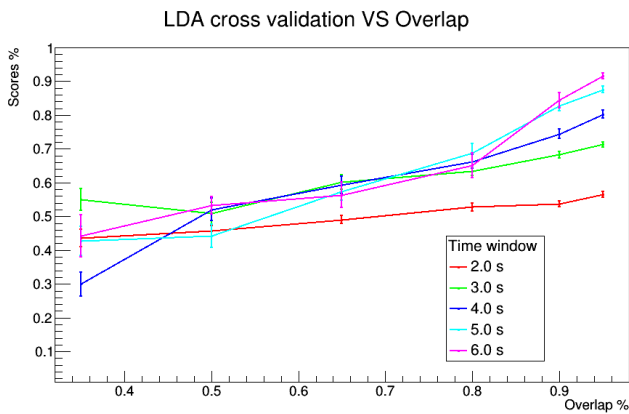


Fig. 3.3: Cross validation accuracy of LDA as a function of the overlap percentages for each time window.

Table 3.3: Relative improvement of the Logistic Regression classifier on Linear Discriminant Analysis.

Window	LDA	LR	Improvement
2.0 s	59.4%	58.8%	-1.0%
3.0 s	69.6%	73.8%	6.0%
4.0 s	76.3%	81.7%	7.1%
5.0 s	89.2%	93.3%	4.6%
6.0 s	90.7%	96.9%	6.8%

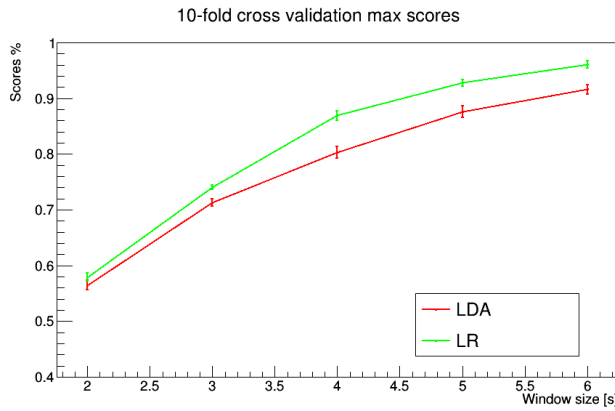


Fig. 3.4: Cross validation accuracy of LDA and LR as a function of the time window using 95% overlap.



Fig. 3.5: Accuracy scores of LDA and LR on the testing dataset as a function of the time window using 95% overlap.

Support vector machine

In this study we only consider the 95% overlap percentage, which has been shown to provide the best results. The training dataset has been used for the optimization of the hyper-parameters of SVM by using the classical ten-fold cross-validation as fitness function of the implemented genetic algorithm. The best parameters reached by the genetic algorithm for each time window are shown in Table 3.4. The trained model has been then validated using the remaining 20% dataset.

The results in terms of the accuracy of the proposed SVM have been com-

Table 3.4: Best SVM parameters achieved by the evolutionary algorithm.

Window	C	γ
2.0 s	59	3.1e-3
3.0 s	689	2.5e-3
4.0 s	28	1.9e-3
5.0 s	79	2.9e-3
6.0 s	187	4.6e-3

pared with the LDA and LR classifier. In particular, the accuracy scores of all methods on testing datasets against the considered time window are shown in Table 3.5. Additionally, Table 3.6 shows the relative improvements of the SVM classifier with respect to LR and LDA [30].

Table 3.5: Accuracy on testing data for the compared classifiers.

Window	LDA	LR	SMV
2.0 s	59.4%	58.8%	74.5%
3.0 s	69.6%	73.8%	85.4%
4.0 s	76.3%	81.7%	92.7%
5.0 s	89.2%	93.3%	95.6%
6.0 s	90.7%	96.9%	97.6%

Table 3.6: Relative improvements of the SVM with respect to LR and LDA.

Window	LDA	LR
2.0 s	25.4%	26.7%
3.0 s	22.7%	15.7%
4.0 s	21.5%	13.5%
5.0 s	7.2%	2.5%
6.0 s	7.6%	0.7%
Average	16.9%	11.8%

3.2 Trainless system validation

3.2.1 Dataset acquisition

Experimental setup

Data was acquired from five volunteers aged from 23 to 40 years. Participants were equipped with the 3D printed headset hosting the FPz, Oz and DRL electrodes, and the Moverio BT-200 Augmented Reality (AR) smart glasses (Fig. 3.6). The latter served as stimulation unit. The AR environment consisted of two white squares positioned at the left and right ends of the screen. The flickering frequencies were generated with the OpenGL library, using a pulsed sinusoidal modulation of the brightness to overcome the limits imposed by the refresh rate 2.2.4. The chosen flickering frequencies were 9 Hz and 10 Hz for the left and right squares respectively. The perceived screen size of the glasses was 80 inches at 5 m projected distance, with a refresh rate of 60 Hz.



Fig. 3.6: The Moverio BT-200 smart glasses.

Experimental protocol

Each volunteer was asked to focus on one stimulus out of two at a time, for 16 s each. Additional 16 s of data have been acquired as background signals, where users were left free to blink one, two, or three consecutive times their eyes without focusing on any of the two stimuli. The resulting dataset consisted of 15 recordings of 16 seconds each for a total of 61440 samples.

3.2.2 Validation procedure

The acquired data was processed to find the best combinations of T , T_A and T_B (a detailed description of the parameters is provided in Sec. 2.3.3). Each signal fragment of length T has been filtered using a 5th-order Butterworth passband filter between 5 Hz and 25 Hz. We then evaluated the Pearson correlation coefficients between the filtered data D_T and two sine

waveform with frequencies 9 Hz and 10 Hz respectively. Based on the algorithm recognition logic, accuracies and response times were evaluated for different combinations of T , T_A and T_B .

The whole dataset was processed using different time windows T in the range 0.3 s - 1.0 s evaluating, for each of them, the features F_A and F_B . An example of distribution of the recognition times for the 9 Hz stimulus is shown in Figure 4. To evaluate the mean response time we fitted the data with an halfnormal distribution.

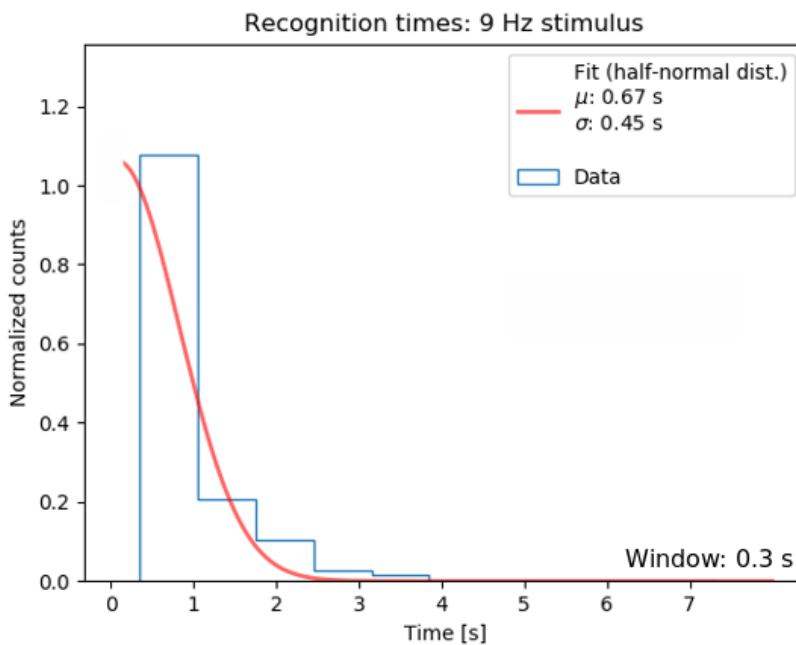


Fig. 3.7: Distribution of the recognition times for the 9 Hz stimulus using a 0.3 s time window. The red line is the half-normal fit to the data.

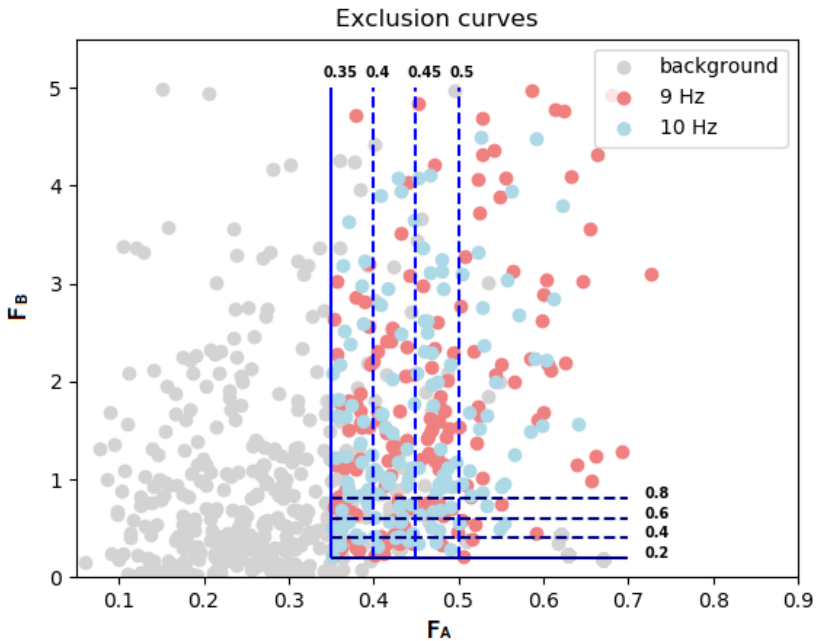


Fig. 3.8: Scatter plot of the features F_A and F_B as defined in Sec. 2.3.3 and exclusion curves using different threshold values T_A and T_B (vertical and horizontal lines respectively).

3.2.3 Results

A first look at the scatter plot in Fig. 3.8, indicates that increasing threshold values T_A and T_B (vertical and horizontal lines respectively) improves the discrimination between background signals (grey dots) and proper signals (red and blue dots), but also increases the total amount of rejected data. This translates into increasing accuracy and decreasing response speed. We fixed the threshold value $T_B = 0.5$ (which means that the correlation with a sine waveform is 50% greater than the other), and then we varied T_A for each time window. The obtained performances in terms of accuracy and response time are shown in Fig. 3.9 and 3.10. The numerical values are shown in Table 3.7.

Using a 1 s time window and $T_A = 0.5$, we reached an accuracy of 99.85% with a response time of 2.36 ± 1.07 s.

On the other hand, we can increase the speed using shorter time windows (down to 0.3 s), at the expense of the accuracy that can go down to 68%.

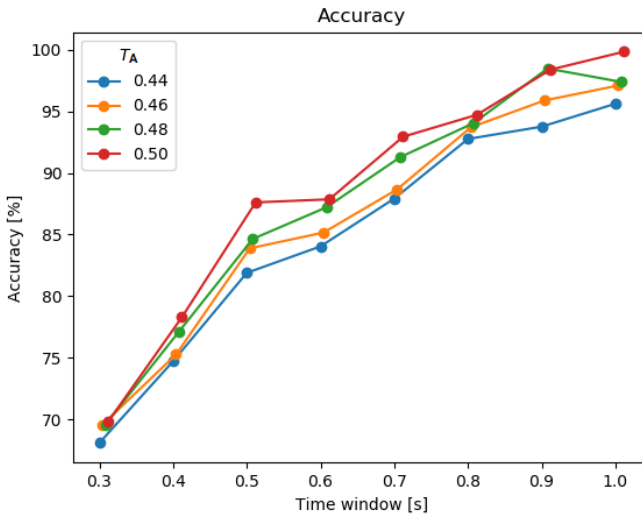
Table 3.7: Analysis results.

$T_A \downarrow / T(s) \rightarrow$	0.3	0.4	0.5	0.6	0.7	0.8	0.9	1.0
0.44	0.71 ± 0.34	0.85 ± 0.40	0.88 ± 0.40	1.07 ± 0.50	1.24 ± 0.57	1.60 ± 0.76	1.69 ± 0.80	1.77 ± 0.82
0.46	0.78 ± 0.38	0.98 ± 0.48	1.00 ± 0.47	1.22 ± 0.58	1.31 ± 0.61	1.67 ± 0.80	1.79 ± 0.85	1.94 ± 0.91
0.48	0.87 ± 0.43	1.02 ± 0.50	1.20 ± 0.58	1.45 ± 0.71	1.43 ± 0.67	1.58 ± 0.75	1.85 ± 0.88	2.15 ± 0.95
0.50	0.96 ± 0.47	1.17 ± 0.58	1.30 ± 0.63	1.59 ± 0.78	1.68 ± 0.81	1.89 ± 0.91	1.91 ± 0.90	2.36 ± 1.07

Response times for different time windows T and threshold values T_A , with $T_B = 0.5$

$T_A \downarrow / T(s) \rightarrow$	0.3	0.4	0.5	0.6	0.7	0.8	0.9	1.0
0.44	68.08%	74.71%	81.89%	84.04%	87.92%	92.76%	93.76%	95.62%
0.46	69.55%	75.26%	83.88%	85.16%	88.67%	93.71%	95.89%	97.10%
0.48	69.57%	77.12%	84.64%	87.21%	91.28%	94.06%	98.48%	97.39%
0.50	69.81%	78.29%	87.61%	87.86%	92.94%	94.72%	98.39%	99.85%

Accuracy for different time windows T and threshold values T_A , with $T_B = 0.5$

**Fig. 3.9:** System accuracy for different threshold values T_A as a function of the time window T .

The eyeblink detection performance has been validated as well. Using the algorithm described in the previous section we successfully detected and counted all the artifacts in the data.

The system was also successfully validated in a live session to control a robotic arm. The live task is described in the next chapter, where some applications of the developed prototype are presented.

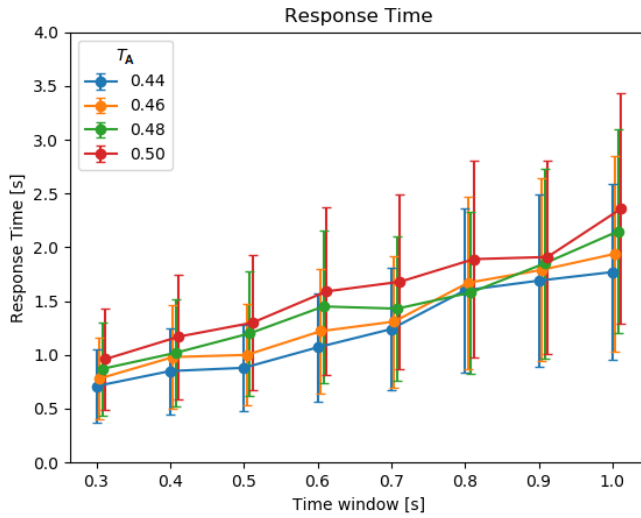


Fig. 3.10: System response time for different threshold values T_A as a function of the time window T .

Chapter 4

APPLICATIONS

SSVEP-based BCIs have been used in many applications in the last years, from home appliances control to spelling systems, video-games, robots, quadcopters and prosthesis control [32, 33, 34, 35, 36, 37]. In a recent work [38], for example, a robotic arm has been controlled using a 10-channels SSVEP-based BCI reaching an accuracy of 92.78% and 4 s response time. In this chapter some applications that can be realized with the developed BCI prototype are presented. Some of them have only been implemented but not tested live due to the lack of volunteers at the time of development.

4.1 Smart wheelchair

Due to their high signal to noise ratio (SNR) and fast time response, SSVEPs are ranked among the fastest and most immediate signals currently available in BCI systems. For these reasons they represent an optimal choice for the realization of assistive devices, since no particular effort is required by the users. Motor disabled people like wheelchair users may benefit from such a BCI system for example to drive the wheelchair itself or to control external devices, substituting the manual control. In this section a cost-effective, brain computer interface (BCI) integrated with the Alexa framework to control multiple devices is presented.



Fig. 4.1: Wheelchair equipped with the BCI system and the User Interface.

The system, developed at the QUASAR laboratories at the Federico II University of Naples, enables wheelchair users to control the ON/OFF state of four Internet-of-Things (IoT) devices promoting independent and autonomous living. A picture of the BCI-equipped smart wheelchair is shown in Fig. 4.1.

4.1.1 Architecture

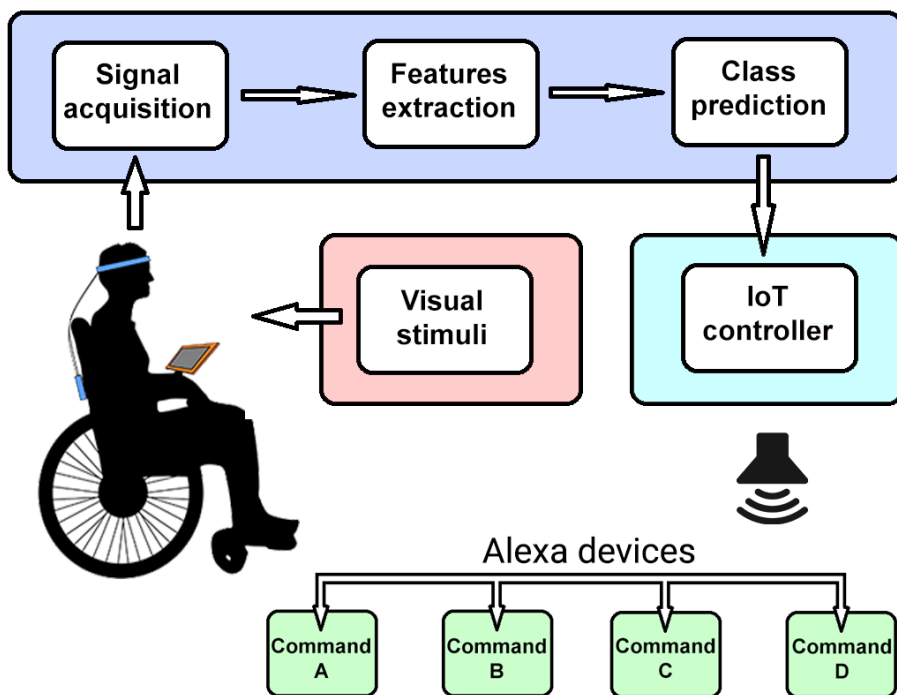


Fig. 4.2: Architecture of the Wheelchair-BCI system.

The architecture of the proposed wheelchair-BCI system is shown in Fig. 4.2. It comprises three modules:

- The developed BCI prototype (Sec. 2), with train-based algorithms enabled, mounted on the back of the wheelchair.
- The stimulation platform, implemented on a 7" android tablet. The stimuli frequencies are 8.57Hz, 10Hz, 12Hz and 15Hz.
- An IoT controller, that translates the recognized stimuli into commands for the Alexa framework. It is written in python and accept

as input the class of the recognized frequency. Thanks to the *gTTS* and *playsound* libraries, each class trigger the vocal synthesis of the statement to control an Alexa-compatible device. As an example, the recognition of the 10 Hz stimulus produces the following outputs: 1) "Alexa, turn on the light", 2) "Alexa, turn off the light". Statement 1) or 2) is chosen based on the previous state.

4.2 Virtual reality

Recent studies [39, 40] suggest that realistic immersive virtual reality (VR) environments, combined with BCI, can be used to improve cognitive functions and social skills in people affected by Autism Spectrum Disorder (ASD). Fixed-frequency flickering images induce synchronous responses in the subject's brain. Using the BCI technology, it is possible to recognize which stimulus the subject is looking at, providing a feedback on his local attention. SSVEP signals have been recently adopted to investigate lateral inhibitions in people affected by ASD, suggesting a correlation between different ASD symptoms and brain responses [41]. The combined use of BCI and VR is very promising for the treatment of autistic children, enforcing the attention deficits and providing novel means of communication, especially in game-like environment where visual feedback are provided to the subject based on his actual attention [42].

In this section an interactive smartphone-based VR environment equipped with a single-channel SSVEP-based EEG-BCI system is presented. Main goal is to provide a high-accuracy, fast-training and cost-effective device for the rehabilitation of ASD children.

4.2.1 Architecture

The system architecture is shown in Fig. 4.3. A VR smartphone-based headset renders the virtual environment providing visual stimuli to the subject. The headset also hosts the three EEG electrodes for acquiring brain signals. A processing unit is responsible for the analysis of the digitized data, extraction of the relevant features and recognition of the observed stimuli. These components, together, form a closed loop: the VR headset provide visual stimuli to the subject; the digitizer captures EEG signals from the electrodes transferring them to the processing unit, which finally analyze the data and sends wireless commands back to the VR environment. The main interface is shown in Fig. 4.4.

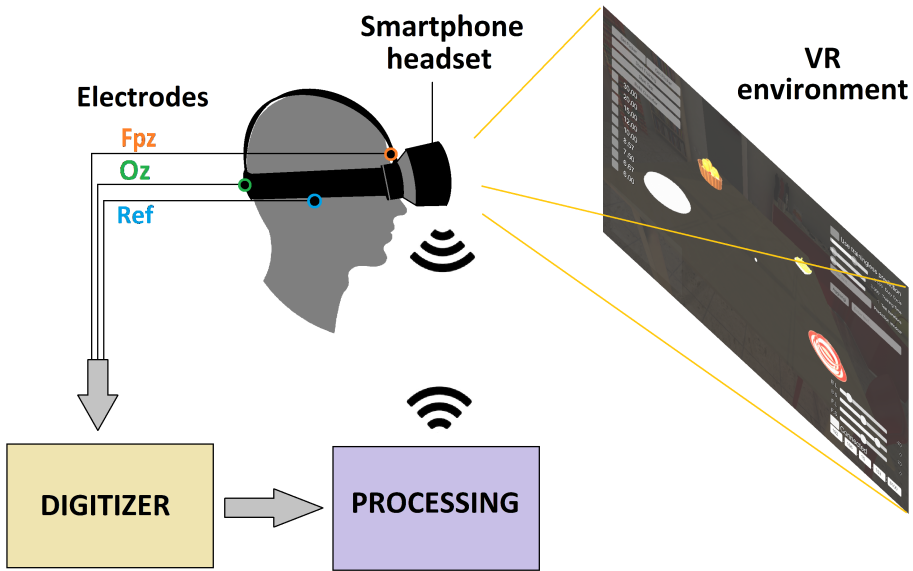


Fig. 4.3: Architecture of the VR-BCI system.



Fig. 4.4: Main interface of the virtual environment.

The VR environment has been developed in collaboration with the Protom Group S.p.A., using the Unity cross-platform game engine. The 3D scenario is a kitchen, with four common-use objects placed on a table as visual stimuli. The luminosity and saturation can be separately adjusted for

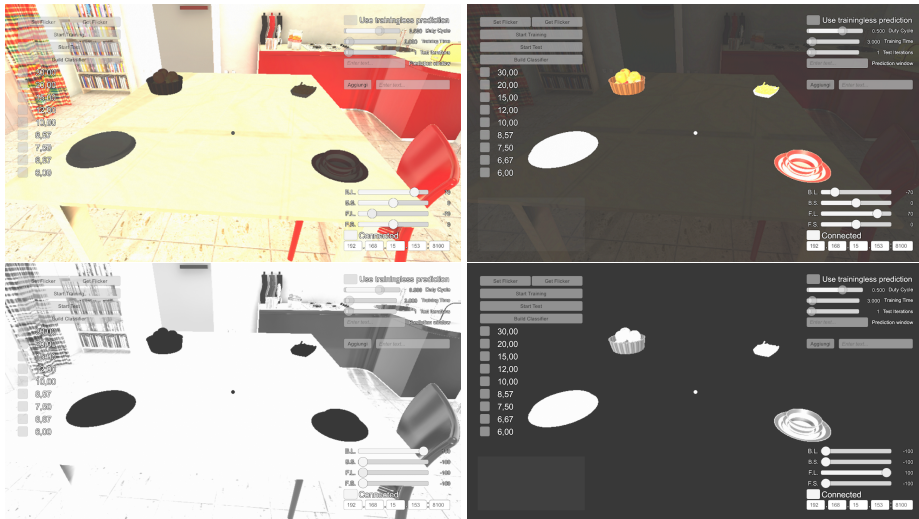


Fig. 4.5: Different configurations of background and stimuli objects in the main scenario.

both the objects and the background. Some examples of different environment configurations are shown in Fig. 4.5. Flickering frequencies can be chosen from an automatically generated list, whose values depend on the device. In fact, the number of the producible frequencies are limited to integer divisors of the monitor refresh rate.

4.3 Robotic arm control

The combined use of Augmented Reality (AR) glasses and a single channel EEG-BCI, based on Steady-State Visual Evoked Potentials (SSVEP) and eye-blink artifacts detection, has been used to control a 6-degrees of freedom robotic arm at the European Organization for Nuclear Research (CERN) robotics facility.

4.3.1 Architecture

The concept design of the developed system is shown in Fig. 4.6. A pair of AR glasses renders the visual stimuli, eliciting SSVEP responses in the subject. Signals are captured through EEG electrodes positioned on the scalp and sent to a processing unit. The elaborated response is sent back to the AR glasses providing a visual feedback to the user and forwarding the related command to a robotic arm.

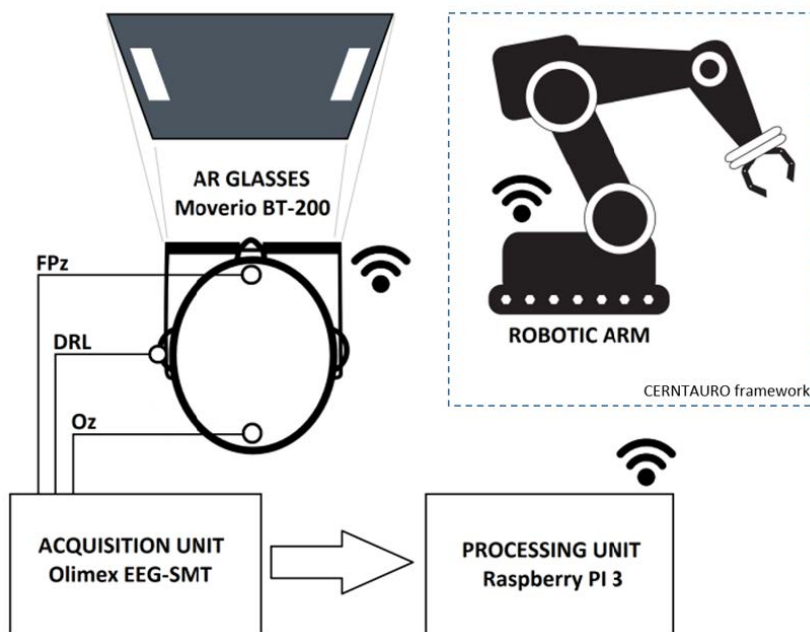


Fig. 4.6: Architecture of the AR-BCI system.

Based on the deep experience accumulated during the last years at CERN operating robots for remote inspection and maintenance [43], we chose to use only two stimuli to reduce the visual fatigue of the operator, increas-

ing the user attention and, consequently, the accuracy of the system. The number of available commands was compensated using the eye-blink detection.

A minimal use of the robotic arm should embrace at least 3-D movements in the space and the control of a gripper. Indicating with x_1 , x_2 , and x_3 the axis of a Cartesian reference system, we used the brain SSVEP responses to move the arm along a fixed axis, and a double eye-blink to change axis. Three consecutive eye-blinks were used to commute the state of the gripper, from open to close and vice versa.

The system is composed of three units:

- The stimulation unit, realized using the Moverio BT-200 AR smart glasses, showing two pulsed sinusoidal waveforms at the left and right ends of the screen. The chosen flickering frequencies are 9 Hz and 10 Hz for the left and right squares respectively. The BT-200 controller also acted as a bridge between the processing unit and the robotic arm.
- The developed BCI prototype (Sec. 2) with trainless algorithm enabled.
- The robotic arm, consisting of a 6-DoF Schunk Powerball arm, already used for intervention in harsh environment by the CERN [44] [43], equipped with a Robotiq 2F-85 adaptive gripper, providing through the CERN Robotic Framework an efficient and unified control interface. To simplify the control of the arm its orientation was kept fixed. Only the end effector position and the gripper state were controlled. The arm movements were controlled in position. The controller was connected through WiFi to the Moverio smart glasses retrieving information in a *JSON* format [45], forwarded from the Raspberry Pi server. This setup allowed the operator to perform the desired picking tasks in a 3D reference system.

4.3.2 Live tests

The online validation consisted in grabbing an object in one position and move it to another, with the robotic arm. The arm was controlled by mapping the brain activities as follows:

- 9 Hz : move backward (along the current axis)
- 10 Hz : move forward (along the current axis)

- 2 blink : change axis ($x_i \leftrightarrow x_j$)
- 3 blink : commute grip

For this task we chose the parameters $T_A = 0.44$, $T_B = 0.5$, and $T = 0.5$ (see Sec. 3.2.3), which gave us an accuracy of 81.9% and a response time of 0.88 ± 0.40 s in the offline analysis. The online task is schematized in Fig. 4.7. Starting from initial position (start), the arm was controlled to pick up the object in position 1 and move it in position 2. The task was completed in less than 100 seconds (comprising the time elapsed to open/close the grip) counting 85 commands. In Fig. 4.8 is shown a picture of the robotic arm controlled by the developed prototype during a live session.

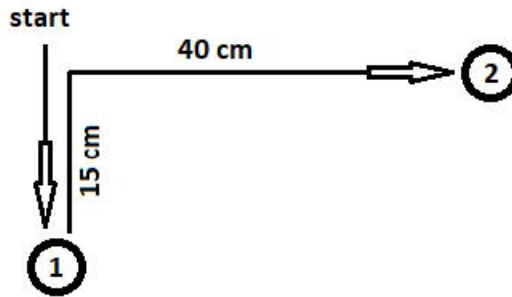


Fig. 4.7: Schematic of the path carried out by the robotic arm during the online task.



Fig. 4.8: Picture of the BCI-controlled robotic arm during an online test session.

CONCLUSIONS

Currently there are many players involved in BCI technology including universities and companies, and significant progress has been made so far. However, the main challenge is to integrate it into real-life applications.

This work demonstrates that this goal can be achieved, both from the hardware and software point of view. In particular, the developed prototype has the potential to be reformulated into an effective and scalable product at the market level. Thanks to the use of a single acquisition channel, by means of dry active electrodes, the prototype turns out to be of extremely practical use. Furthermore, the combined use of SSVEP potentials with different brain signals makes this technology extremely flexible, increasing its capabilities.

Machine learning plays a key role in signal recognition, especially in obtaining information from particularly noisy signals that encode numerous classes. In particular, the use of Support Vector Machines (SVM) and Evolutionary Algorithms improved noticeably the accuracy of the system with respect to the state of the art approaches for single channel SSVEP based BCIs, in distinguishing between four classes. On the other hand, when few classes are involved, the use of a correlation based algorithm also proved to be efficient, being able to effectively control a 6-DoF robotic arm.

The applications covered in the last chapter are just an example of the potential of this technology. Part of them are still under investigation while others, such as spelling systems and selection of questionnaire answers, are under development. The research on novel BCIs in the medical field is of particular interest, since most EEG diagnostic devices are very expensive, invasive, and available only in dedicated facilities. Conversely, the portable framework studied in this work is well suited for the continuous monitoring of brain signals in home and primary care. However, there is currently a lack of commercial devices that are tailored for these scenarios.

It is expected that technologies based on EEG-BCIs will be integrated in applications that ranges from diagnostics to entertainment. In particular, a

portable framework enhanced by machine learning techniques may play a crucial role where extremely low latency and rapid training are mandatory.

REFERENCES

- [1] A. Hodgkin and A. Huxley, "Action potentials recorded from inside a nerve fibre," *Nature*, vol. 144, pp. 710 – 711, 1939.
- [2] D. Pelvig, H. Pakkenberg, A. Stark, and B. Pakkenberg, "Neocortical glial cell numbers in human brains," *Neurobiology of Aging*, vol. 29, no. 11, pp. 1754–1762, 2008.
- [3] P. Kerr, A. Caputy, and N. Horwitz, "A history of cerebral localization," *Neurosurg Focus*, 2005.
- [4] G. Fritsch and E. Hitzig, "Electric excitability of the cerebrum (uber die elektrische erregbarkeit des grosshirns)," *Epilepsy Behav.*, 2009 (1870).
- [5] S. Michael, "One century of brain mapping using brodmann areas," *Clinical Neuroradiology*, 2009.
- [6] C. Bouckaert, S. Vandenberghe, and R. V. Holen, "Evaluation of a compact, high-resolution SPECT detector based on digital silicon photomultipliers," *Physics in Medicine and Biology*, vol. 59, no. 23, pp. 7521–7539, 2014.
- [7] D. Bailey, J. Karp, and S. Surti, *Physics and Instrumentation in PET*. Springer, 2005.
- [8] H. Weinstock, "Squid sensors: fundamentals, fabrication and applications," 2012.
- [9] E. Amaro Jr and G. J. Barker, "Study design in fmri: basic principles," *Brain and cognition*, vol. 60, no. 3, pp. 220–232, 2006.
- [10] S. Coyle, T. Ward, C. Markham, and G. McDarby, "On the suitability of near-infrared (nir) systems for next-generation brain–computer interfaces," *Physiological measurement*, vol. 25, no. 4, p. 815, 2004.

-
- [11] E. C. Leuthardt, K. J. Miller, G. Schalk, R. P. Rao, and J. G. Ojemann, "Electrocorticography-based brain computer interface-the seattle experience," *IEEE Transactions on Neural Systems and Rehabilitation Engineering*, vol. 14, no. 2, pp. 194–198, 2006.
- [12] K. J. Miller, P. Shenoy, J. W. Miller, R. P. Rao, J. G. Ojemann *et al.*, "Real-time functional brain mapping using electrocorticography," *Neuroimage*, vol. 37, no. 2, pp. 504–507, 2007.
- [13] M. Hill, E. Rios, S. K. Sudhakar, D. H. Roossien, C. Caldwell, D. Cai, O. J. Ahmed, S. F. Lempka, and C. A. Chestek, "Quantitative simulation of extracellular single unit recording from the surface of cortex," *Journal of neural engineering*, vol. 15, no. 5, p. 056007, 2018.
- [14] H. Berger, "Über das elektroencephalogramm des menschen," *Archiv f. Psychiatrie*, vol. 87, p. 527 – 570, 1929.
- [15] J. N. Acharya, A. J. Hani, J. Cheek, P. Thirumala, and T. N. Tsuchida, "American clinical neurophysiology society guideline 2: guidelines for standard electrode position nomenclature," *The Neurodiagnostic Journal*, vol. 56, no. 4, pp. 245–252, 2016.
- [16] N. G. Tavares and R. Gad, "Steady-state visual evoked potential-based real-time bci for smart appliance control," in *Cognitive Informatics and Soft Computing*. Springer, 2019, pp. 795–805.
- [17] J. Polich, "Updating p300: an integrative theory of p3a and p3b," *Clinical neurophysiology*, vol. 118, no. 10, pp. 2128–2148, 2007.
- [18] E. A. Mohamed, M. Z. Yusoff, A. S. Malik, M. R. Bahloul, D. M. Adam, and I. K. Adam, "Comparison of eeg signal decomposition methods in classification of motor-imagery bci," *Multimedia Tools and Applications*, vol. 77, no. 16, pp. 21305–21327, 2018.
- [19] G. Garipelli, R. Chavarriaga, and J. del R Millán, "Single trial analysis of slow cortical potentials: a study on anticipation related potentials," *Journal of neural engineering*, vol. 10, no. 3, p. 036014, 2013.
- [20] J. J. Vidal, "Toward direct brain-computer communication," *Annual Review of Biophysics and Bioengineering*, vol. 2, no. 1, pp. 157–180, 1973.
- [21] J. R. Wolpaw, N. Birbaumer, D. J. McFarland, G. Pfurtscheller, and T. M. Vaughan, "Brain–computer interfaces for communication and control," *Clinical Neurophysiology*, vol. 113, no. 6, pp. 767–791, 2002.

-
- [22] H. Cecotti, I. Volosyak, and A. Gräser, “Reliable visual stimuli on lcd screens for ssvep based bci,” in *2010 18th European Signal Processing Conference*, Aug 2010, pp. 919–923.
- [23] J. W. Cooley and J. W. Tukey, “An algorithm for the machine calculation of complex fourier series,” *Mathematics of Computation*, vol. 19, no. 90, pp. 297–301, 1965.
- [24] D. W. Hosmer and S. Lemeshow, *Applied logistic regression (Wiley Series in probability and statistics)*, 2nd ed. Wiley-Interscience Publication, 2000.
- [25] S. Raschka, *Python Machine Learning*. Packt Publishing, 2015.
- [26] C. Cortes and V. Vapnik, “Support-vector networks,” *Machine Learning*, vol. 20, pp. 273 – 297, 1995.
- [27] G. Acampora, P. Trinchese, and A. Vitiello, “A dataset of eeg signals from a single-channel ssvep-based brain computer interface,” *Data in Brief*, vol. 35, p. 106826, 2021.
- [28] A. Luo and T. J. Sullivan, “A user-friendly ssvep-based brain–computer interface using a time-domain classifier,” *Journal of Neural Engineering*, vol. 7, no. 2, p. 026010, 2010.
- [29] G. Acampora, P. Avella, V. Loia, S. Salerno, and A. Vitiello, “Improving ontology alignment through memetic algorithms,” in *2011 IEEE International Conference on Fuzzy Systems (FUZZ-IEEE 2011)*. IEEE, 2011, pp. 1783–1790.
- [30] G. Acampora, P. Trinchese, and A. Vitiello, “Classifying eeg signals in single-channel ssvep-based bcis through support vector machine,” in *2020 IEEE International Conference on Systems, Man, and Cybernetics (SMC)*. IEEE, 2020, pp. 2305–2310.
- [31] G. Acampora, P. Trinchese, and A. Vitiello, “Applying logistic regression for classification in single-channel ssvep-based bcis,” in *2020 IEEE International Conference on Systems, Man, and Cybernetics (SMC)*. IEEE, 2019, pp. 33–38.
- [32] S. F. Anindya, H. H. Rachmat, and E. Sutjiredjeki, “A prototype of ssvep-based bci for home appliances control,” in *2016 1st International Conference on Biomedical Engineering (IBIOMED)*, Oct 2016, pp. 1–6.

-
- [33] E. Yin, Z. Zhou, J. Jiang, Y. Yu, and D. Hu, "A dynamically optimized ssvep brain-computer interface (bci) speller," *IEEE Transactions on Biomedical Engineering*, vol. 62, no. 6, pp. 1447–1456, June 2015.
- [34] I. Martišius and R. Damaševičius, "A prototype ssvep based real time bci gaming system," *Computational Intelligence and Neuroscience*, vol. 2016, p. 15, 2016.
- [35] A. Astaras, N. Moustakas, A. Athanasiou, and A. Gougoussis, "Towards brain-computer interface control of a 6-degree-of-freedom robotic arm using dry eeg electrodes," *Advances in Human-Computer Interaction*, vol. 2013, 05 2013.
- [36] G. R. Muller-Putz and G. Pfurtscheller, "Control of an electrical prosthesis with an ssvep-based bci," *IEEE Transactions on Biomedical Engineering*, vol. 55, no. 1, pp. 361–364, Jan 2008.
- [37] M. Wang, R. Li, R. Zhang, G. Li, and D. Zhang, "A wearable ssvep-based bci system for quadcopter control using head-mounted device," *IEEE Access*, vol. 6, pp. 26 789–26 798, 2018.
- [38] X. Chen, B. Zhao, Y. Wang, S. Xu, and X. Gao, "Control of a 7-dof robotic arm system with an ssvep-based bci," *International Journal of Neural Systems*, vol. 28, no. 08, p. 1850018, 2018.
- [39] N. Didehbani, T. Allen, M. Kandalaft, D. Krawczyk, and S. Chapman, "Virtual reality social cognition training for children with high functioning autism," *Computers in Human Behavior*, vol. 62, pp. 703 – 711, 2016.
- [40] A. L. Wainer and B. R. Ingersoll, "The use of innovative computer technology for teaching social communication to individuals with autism spectrum disorders," *Research in Autism Spectrum Disorders*, vol. 5, no. 1, pp. 96 – 107, 2011.
- [41] A. Dickinson, R. Gomez, M. Jones, V. Zemon, and E. Milne, "Lateral inhibition in the autism spectrum: An ssvep study of visual cortical lateral interactions," *Neuropsychologia*, vol. 111, pp. 369 – 376, 2018.
- [42] E. V. C. Friedrich, N. Suttie, A. Sivanathan, T. Lim, S. Louchart, and J. A. Pineda, "Brain-computer interface game applications for combined neurofeedback and biofeedback treatment for children on the autism spectrum," *Frontiers in Neuroengineering*, vol. 7, p. 21, 2014.

- [43] M. D. Castro, M. Ferre, and A. Masi, "Cerntauro: A modular architecture for robotic inspection and telemanipulation in harsh and semi-structured environments," *IEEE Access*, vol. 6, pp. 37 506–37 522, 2018.
- [44] C. Lefevre, "The cern accelerator complex," Tech. Rep., 2008.
- [45] F. Pezoa, J. L. Reutter, F. Suarez, M. Ugarte, and D. Vrgoč, "Foundations of json schema," in *Proceedings of the 25th International Conference on World Wide Web*, 2016, pp. 263–273.